Vol 18 No 3, March 2009
1674-1056/2009/18(03)/1127-09
Chinese Physics B
© 2009 Chin. Phys. Soc.
and IOP Publishing Ltd

The numerical study of shock-induced hydrodynamic instability and mixing*

Wang Tao(王 涛)[a)†], Bai Jing-Song(柏劲松)[a)b)],
Li Ping(李 平)[a)b)], and Zhong Min(钟 敏)[a)]

[a)] *Institute of Fluid Physics, China Academy of Engineering Physics, Mianyang* 621900, *China*

[b)] *National Laboratory for Shock Wave and Detonation Physics Research, Institute of Fluid Physics, China Academy of Engineering Physics, Mianyang* 621900, *China*

(Received 1 January 2008; revised manuscript received 4 August 2008)

Based on multi-fluid volume fraction and piecewise parabolic method (PPM), a multi-viscosity-fluid hydrodynamic code MVPPM (Multi-Viscosity-Fluid Piecewise Parabolic Method) is developed and applied to the problems of shock-induced hydrodynamic interfacial instability and mixing. Simulations of gas/liquid interface instability show that the influences of initial perturbations on the fluid mixing zone (FMZ) growth are significant, especially at the late stages, while grids have only a slight effect on the FMZ width, when the interface is impulsively accelerated by a shock wave passing through it. A numerical study of the hydrodynamic interfacial instability and mixing of gaseous flows impacted by re-shocks is presented. It reveals that the numerical results are in good agreement with the experimental results and the mixing growth rate strongly depends on initial conditions. Ultimately, the jelly layer experiment relevant to the instability impacted by exploding is simulated. The shape of jelly interface, position of front face of jelly layer, crest and trough of perturbation versus time are given; their simulated results are in good agreement with experimental results.

Keywords: interfacial instability, mixing, multi-fluid hydrodynamic, volume fraction
PACC: 4720, 4620

1. Introduction

The instability of a material interface interacting with an incident shock was predicted theoretically by Richtmyer in 1960,[1] and confirmed experimentally by Meshkov[2] ten years later. Since then, this interfacial instability has been known as the Richtmyer–Meshkov (RM) instability. The RM instability is closely related to the Rayleigh–Taylor (RT) instability,[3−5] which is an interfacial instability between two fluids with different densities, driven by an external force. The RM and RT instabilities share some common features, such as the formation and growth of bubbles and spikes. The 'light' fluid penetrates into "heavy" fluid as bubbles, while the 'heavy' fluid enters the "light" fluid as spikes. However, the dynamics of RM instability is qualitatively different from that of RT instability. A small initial perturbation to the interface separating the two fluids with different densities grows linearly first, and nonlinearly develops at the late time, and subsequently transits to turbulence. Linear stability theory has achieved excellent results in linear growth stage, while there exist more obstacles to the investigation of nonlinear and turbulent mixing stages at present. Many scientists have devoted themselves to this field and gained good achievements.[6−11]

The RM instability is of importance in fields ranging from astrophysics to combustion. For instance, the RM instability is believed to occur when the outward propagating shock wave generated by the collapsing core of a dying star passes over the helium–hydrogen interface.[12] The RM instability is also of critical importance to inertial confinement fusion (ICF), in which the shell that encapsulates the deuterium-tritium fuel becomes RM unstable as it is accelerated inward by the ablation of its outer surface by laser or secondary x-ray radiation. The RM instability is also important to high-speed combustion applications, because of greatly enhancing mixing and changing the burning rate. Nevertheless the

*Project supported by the National Natural Science Foundation of China (Grant Nos 10672151 and 10772166), the Foundation of China Academy of Engineering Physics (Grant No 2008B0202011) and the Fundamental Quality and Reliability of National Defence Science and Technology Industry of China.
†E-mail: qinwufeiyang1979@126.com, wtaoxp@21cn.com

presence of shock waves in the RM instability significantly complicates its study theoretically, numerically and experimentally. In the present paper, the flow mixing induced by the RM instabilities is researched numerically by using the multi-viscosity-fluid piecewise parabolic method (MVPPM)[13] code, which is developed from the Euler code of multi-fluid piecewise parabolic method) (MFPPM).[14,15] The code is verified by comparing the numerical results and the experimental results, and the evolution of instability is analysed. It should be noted that only the molecular dynamics viscosity is considered in the simulations, so the code MVPPM cannot simulate the turbulence accurately, that is why we name the fluid mixing zone (FMZ) rather than prevailing turbulent mixing zone (TMZ).

2. Algorithm

2.1. Basic equations

On the basis of volume fraction model,[16] we combine the piecewise parabolic method (PPM) with the interface tracking technique to solve the hydrodynamic equations, and to study the hydrodynamic instability. With the viscosity and heat-transfer taken into account, the governing equations can be written as follows:

$$\begin{aligned}
&\frac{\partial \rho}{\partial t}+\frac{\partial \rho u_j}{\partial x_j}=0,\\
&\frac{\partial \rho u_i}{\partial t}+\frac{\partial \rho u_j u_i}{\partial x_j}=-\frac{\partial p}{\partial x_i}+\frac{\partial \sigma_{ij}}{\partial x_j},\\
&\frac{\partial \rho E}{\partial t}+\frac{\partial\left(\rho u_j E+p u_j\right)}{\partial x_j}=-\frac{\partial q_j}{\partial x_j}+\frac{\partial\left(u_i \sigma_{ij}\right)}{\partial x_j},\\
&\frac{\partial Y^{(s)}}{\partial t}+u_j \frac{\partial Y^{(s)}}{\partial x_j}=0, \quad s=1,2,\ldots,N-1.
\end{aligned} \tag{1}$$

Here, i and j represent the three directions of x, y, z respectively; ρ, $u_k(k=i,\ j)$, p are density, speed and pressure of material; E is the total energy per unit mass; N is of the category of material; $Y^{(s)}$ is the volume fraction of the sth material and satisfies $\sum Y^{(s)}=1$. σ_{ij} is the Newtonian fluid viscosity stress tensor, expressed as

$$\sigma_{ij}=\mu\left(\partial u_i/\partial x_j+\partial u_j/\partial x_i-\frac{2}{3}\delta_{ij}\left(\partial u_k/\partial x_k\right)\right), \tag{2}$$

where μ is the fluid viscosity; q_j is the energy flux per unit time and space, $q_j=-\lambda\partial T/\partial x_j$; T is temperature; λ is the efficient heat-transfer coefficient.

The operator splitting technique is used to decompose the physical problems, as described by Eq.(1), into three sub-processes, i.e. the computation of inviscid flux, viscous flux and heat flux, and then Eq.(1) can be decomposed into two equations as follows:

$$\begin{aligned}
&\frac{\partial \rho}{\partial t}+\frac{\partial \rho u_j}{\partial x_j}=0,\\
&\frac{\partial \rho u_i}{\partial t}+\frac{\partial \rho u_j u_i}{\partial x_j}+\frac{\partial p}{\partial x_i}=0,\\
&\frac{\partial \rho E}{\partial t}+\frac{\partial\left(\rho u_j E+p u_j\right)}{\partial x_j}=0,\\
&\frac{\partial Y^{(s)}}{\partial t}+u_j \frac{\partial Y^{(s)}}{\partial x_j}=0, \quad s=1,2,\ldots,N-1,
\end{aligned} \tag{3}$$

and

$$\begin{aligned}
&\frac{\partial \rho}{\partial t}=0,\\
&\frac{\partial \rho u_i}{\partial t}=\frac{\partial \sigma_{ij}}{\partial x_j},\\
&\frac{\partial \rho E}{\partial t}=-\frac{\partial q_j}{\partial x_j}+\frac{\partial\left(u_i \sigma_{ij}\right)}{\partial x_j},\\
&\frac{\partial Y^{(s)}}{\partial t}=0, \qquad s=1,2,...,N-1.
\end{aligned} \tag{4}$$

2.2. Difference scheme

In order to calculate the inviscid flux and capture the interface, third-order precision PPM (two-order precision in time) is combined with volume of fluid (VOF) method[17,18] to solve Euler equation (3). Equation (3) is simplified into multi one-dimensional equations, for example, the 1D equations in the x direction are

$$\begin{aligned}
&\frac{\partial \rho}{\partial t}+\frac{\partial(\rho u)}{\partial x}=0,\\
&\frac{\partial(\rho u)}{\partial t}+\frac{\partial\left(\rho u^2+p\right)}{\partial x}=0,\\
&\frac{\partial(\rho E)}{\partial t}+\frac{\partial(\rho u E+p u)}{\partial x}=0,\\
&\frac{\partial Y^{(s)}}{\partial t}+u\frac{\partial Y^{(s)}}{\partial x}=0, \quad s=1,\ 2,...,\ N-1.
\end{aligned} \tag{5}$$

The two-step Lagrange-remapping algorithm is applied to solving Eq.(5), and one time step calculation can be divided into four steps: (1) the piecewise parabolic interpolation of physical quantities; (2) solving Riemann problems approximately; (3) marching of Lagrange equations; Remapping the physical quantities onto stationary Euler meshes. For the Lagrange step, the substantial derivative of volume fraction $Y^{(s)}$ is zero and unchangeable, and multi-fluid one dimen-

sional Lagrange equations can be written as

$$\begin{aligned}
&\frac{\partial \tau}{\partial t} - \frac{\partial (r^a u)}{\partial m} = 0,\\
&\frac{\partial u}{\partial t} + r^a \frac{\partial p}{\partial m} = 0,\\
&\frac{\partial E}{\partial t} + \frac{\partial (r^a u p)}{\partial m} = 0,\\
&\frac{\partial Y^{(s)}}{\partial t} = 0, \qquad s = 1,\ 2, ...,\ N-1,
\end{aligned} \tag{6}$$

where τ is the specific volume; α is 0, 1, and 2 corresponding to plane, axially symmetric and spherically symmetric problems respectively; r is the spatial coordinate; m is the mass coordinate $m = \int_{r_0}^{r} \rho r^a \mathrm{d}r$. After this step, the meshes have distorted and the average physical quantities in Lagrange coordinates must be remapped back onto Euler meshes, $(\rho^{\mathrm{E}})^{n+1}$, $(u^{\mathrm{E}})^{n+1}$, $(E^{\mathrm{E}})^{n+1}$ and $((Y^{(s)})^{\mathrm{E}})^{n+1}$.

The VOF method, which is a kind of volume tracking technique and also a popular interface tracking algorithm that has been proven to be a useful and robust tool since its development over two decades ago, is used to track the interface. Fluid volume function F is defined as the ratio of fluid volume in each cell to the cell volume, and it is the volume fraction function $Y^{(s)}$, then the following three conditions are possible:

$Y^{(s)} = 0$: the cell is empty (of the sth fluid)

$Y^{(s)} = 1$: the cell is full (of the sth fluid)

$0 < Y^{(s)} < 1$: the cell contains the interface between the sth fluid and one or more other fluids.

All variables and properties are shared by the phase (or fluid) and the represented volume-averaged values. As long as the volume fraction of each phase is known at each location, the variables and properties in any given cell are purely either representative of one of the phase, or representative of a mixed phases, depending on the volume fraction values.

2.3. Dissipation term

For the viscous flux and heat flux, Eq.(4) needs solving based on inviscid flux. We use the second-order spatial centre difference and two-step Rung–Kutta time marching to solve it. Newtonian fluid viscosity stress tensor and energy flux only influence the momentum and the energy of the fluid, so the first equation and the last equation can be neglected, and Eq.(4) can be written as

$$\frac{\partial \bar{U}}{\partial t} + \frac{\partial \bar{F}}{\partial x} + \frac{\partial \bar{G}}{\partial y} + \frac{\partial \bar{H}}{\partial z} = 0 \tag{7}$$

with

$$\begin{aligned}
&\bar{U} = (\rho u, \rho v, \rho w, \rho E)^T,\\
&\bar{F} = (-\sigma_{xx}, -\sigma_{yx}, -\sigma_{zx}, -u\sigma_{xx} - v\sigma_{yx} - w\sigma_{zx} + q_x)^T,\\
&\bar{G} = (-\sigma_{xy}, -\sigma_{yy}, -\sigma_{zy}, -u\sigma_{xy} - v\sigma_{yy} - w\sigma_{zy} + q_y)^T,\\
&\bar{H} = (-\sigma_{xz}, -\sigma_{yz}, -\sigma_{zz}, -u\sigma_{xz} - v\sigma_{yz} - w\sigma_{zz} + q_z)^T.
\end{aligned} \tag{8}$$

In the cartesian coordinates system, the spatial derivative terms in Eq.(7) can be discretized as follows:

$$\begin{aligned}
L_h\left(\bar{U}^E_{i,j,k}\right) =& \frac{\bar{F}^E_{i-1/2,j,k}}{\Delta x} + \frac{\bar{G}^E_{i,j-1/2,k} - \bar{G}^E_{i,j+1/2,k}}{\Delta y}\\
&+ \frac{\bar{H}^E_{i,j,k-1/2} - \bar{H}^E_{i,j,k+1/2}}{\Delta z}.
\end{aligned} \tag{9}$$

The superscript 'E' denotes that the physical quantities are solutions of Euler equations (3). Then Eq.(7) is solved by two Rung–Kutta marching

$$\begin{aligned}
&\bar{U}^{(l)}_{i,j,k} = \bar{U}^E_{i,j,k} + \Delta t L_h\left(\bar{U}^E_{i,j,k}\right),\\
&U^{n+1}_{i,j,k} = \frac{1}{2}\left[\bar{U}^E_{i,j,k} + \bar{U}^{(l)}_{i,j,k} + \Delta t L_h\left(\bar{U}^{(l)}_{i,j,k}\right)\right].
\end{aligned} \tag{10}$$

3. Results and discussion

3.1. Case 1 : instability of gas/liquid interface

The computational model and the initial pressure[19] are presented in Fig.1. On the left of interface is air and on the right is water, the interface is impacted by high-pressure He gas. The experimental apparatus is fixed vertically, and the gravity is negligible, relative to shock wave's accelerating. We set three kinds of initial perturbations to the interface: the first one is a random perturbation; the second one is a natural perturbation (The interface is a concave from left to right); the third one is a point perturbation which is a very small semicircle penetrating into water in the middle of the interface. The computational domain is divided into 1×26 zones each with 100×68 meshes for parallel calculation (26 CPUs).

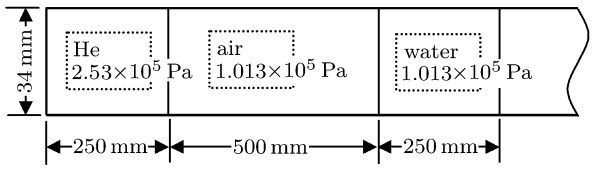


Fig.1. Computational model.

Figures 2(a), 2(b) and 2(c) show the FMZ width, spike width and bubble width versus time respectively. It can be seen that the FMZ width increases with time and is influenced little by initial perturbations at the early time, and the evolution of spike width is similar to that of the FMZ width; the bubble width increases roughly linearly and is affected little by initial perturbations relative to the FMZ or spike width. In fact, the FMZ width is the sum of the bubble width and spike width, and the spike grows faster than the bubble.

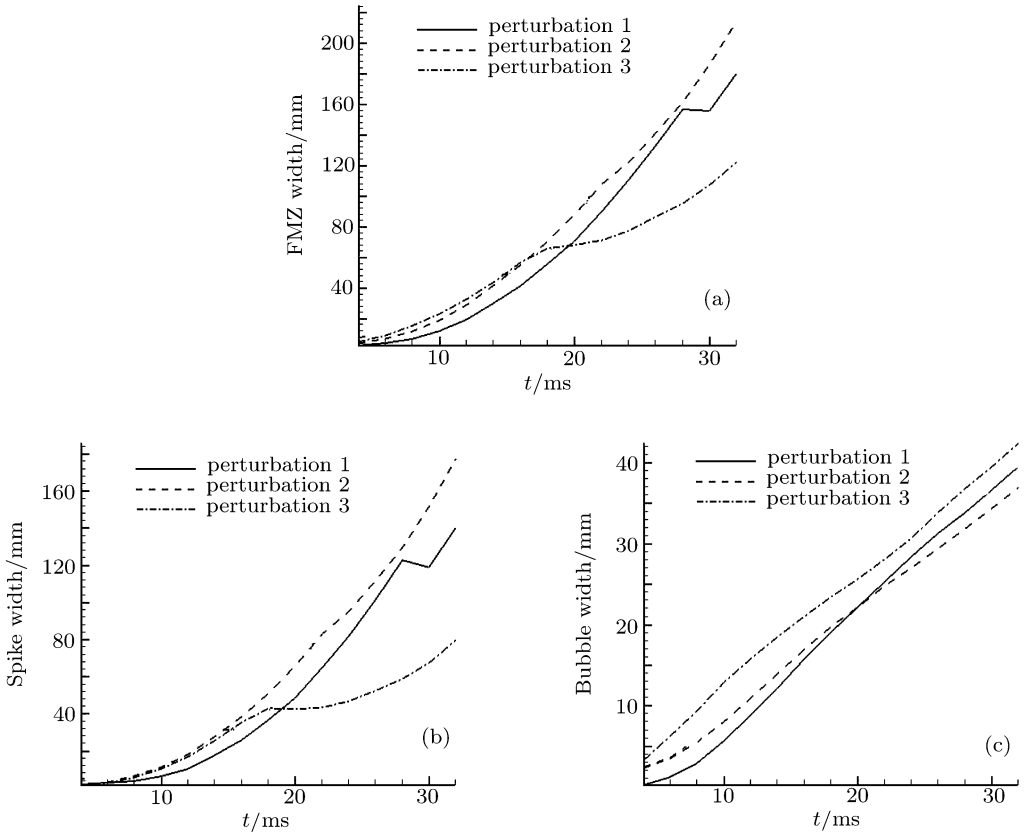


Fig.2. (a) FMZ widths vs time for different perturbations, (b) Spike widths vs time for different perturbations, and (c) Bubble widths vs time for different perturbations.

The configurations of FMZ for different initial perturbations at one time are presented in Fig.3, where on the right is water. It reveals that the configuration of FMZ is dependent on initial perturbation. We have also made the grids finer and found that the effect of grid size is small.



Fig.3. Configurations of FMZ for different initial perturbations at one time.

3.2. Case 2: instability and flow mixing under impaction of re-shocks

The evolution of turbulent mixing zone impacted by a single shock wave has been known well, but it has not been understood deeply yet when impacted by multiple shock waves. The instability and the flow mixing of light/heavy gas interface under impaction of re-shocks[20,21] are simulated. The computational

model is presented in Fig.4. The shock wave Mach number is 1.2, and the left boundary is inflow/outflow and the others are all walls. The computational domain is divided into 36 zones (9×4 CPUs) each with 200×200 meshes for parallel calculating.

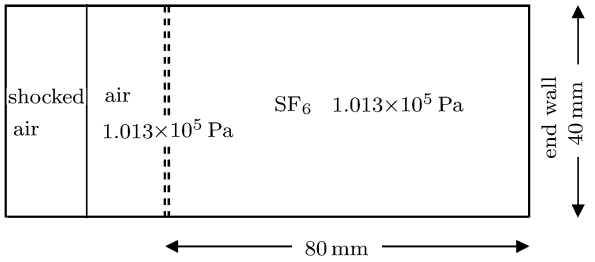


Fig.4. Computational model of shock tube.

The initial perturbation is a random one which is on the interface between air and SF_6 gas (the Atwood number=0.67). It has two forms: (1) the initial amplitude is 0.175 mm, initial wavelength λ is between 0.5 and 6.5 mm, i.e. $0.5 < \lambda < 6.5$ mm, and the initial average wavelength $\langle\lambda\rangle$ is 3.5 mm; (2) the initial amplitude is 0.075 mm, and $0.5 < \lambda < 2.5$ mm, $\langle\lambda\rangle = 1.5$ mm. The initial parameters of materials are shown in Table 1.

Table 1. Initial parameters.

material	ρ/(kg/m^3)	p/Pa	V/(m/s)	γ	μ/(Pa·s)
SF_6	6.5204	1.0×10^5	0.0	1.09	1.72×10^{-5}
unshocked air	1.29	1.0×10^5	0.0	1.4	1.84×10^{-5}
shocked air	1.7307	1.51×10^5	100.66	1.4	1.84×10^{-5}

When the incident shock collides with the material interface, it bifurcates into a transmitted shock and a reflected wave. Depending on the material properties of fluid crossing the material interface and the incident shock strength, the reflected wave can be either a shock or a rarefaction wave.[22] For the majority of real gases, the criterion states that when the shock collides with the material interface from light fluid phase to heavy fluid phase, the reflected wave is a shock; otherwise it is a rarefaction wave. Here the reflected wave is a shock, whereas it cannot affect the evolution of the interface. The transmitted shock hits the endwall and returns to the interface, and then it collides with the material interface again.

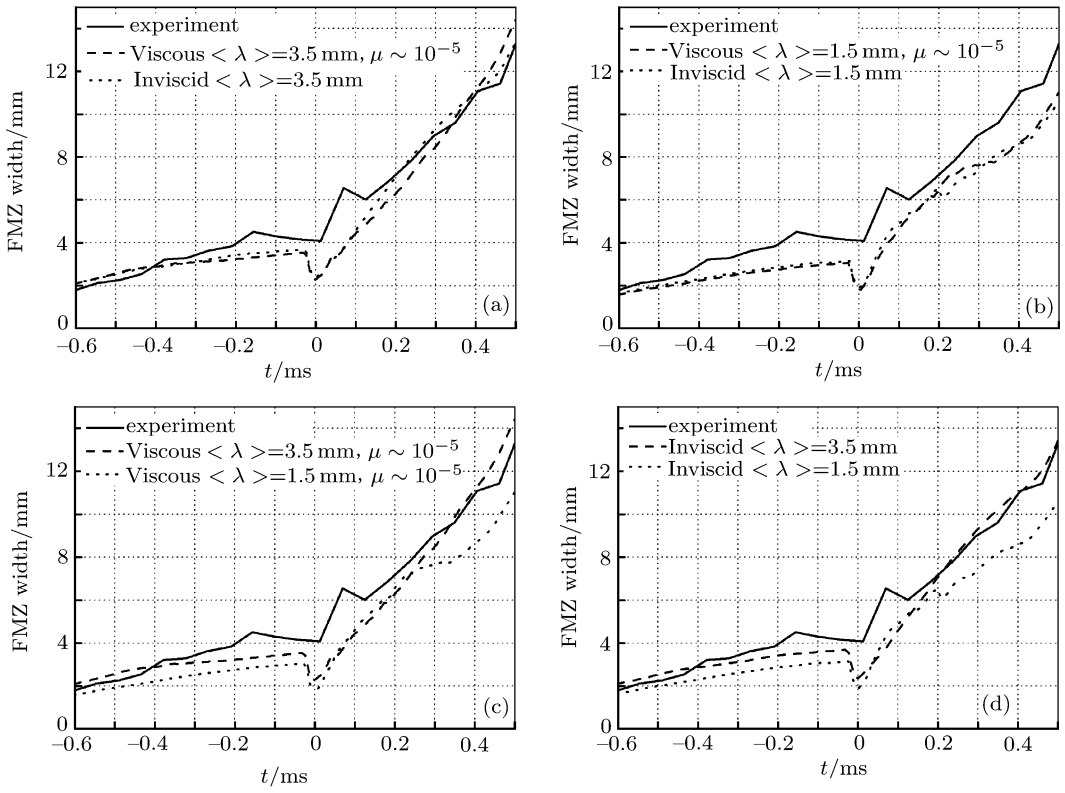


Fig.5. FMZ widths vs time (t=0 denotes the re-shock arrival at the interface).

Figures 5(a)–5(d) show the FMZ width versus time and a comparison between numerical results and experimental results, displaying that FMZ width increases slowly at the early time, because the linear flow plays a dominant role. When the re-shock arrives at the interface and collides with it again, the FMZ width decreases abruptly, which is because the transforming of crest and trough makes it negatively grow. This transformation is the typical characteristics when shock wave travels from heavy fluid phase to light fluid phase.[23] Thenceforth the effect of flow nonlinearity plays a principal role, the rarefaction wave moves back and forth, and weakens gradually, therefore the FMZ growth rate increases sharply. We can also see that the influence of molecular dynamics viscosity is limited, and the largest error is less than 5% between inviscid and viscous results. However, the FMZ growth rate strongly depends on initial conditions (initial spectrum and initial amplitude). It can be seen that the growth rate following the re-shock impacting increases with the initial average wavelength increasing, and numerical results of $\langle\lambda\rangle = 3.5\,\text{mm}$ spectrum are in better agreement with the experimental measurements than those of $\langle\lambda\rangle = 1.5\,\text{mm}$ spectrum.

Figures 6(a)–6(c) present the density distributions at three moments before and after the shock impacting the interface, for the case of initial average wavelength $\langle\lambda\rangle = 3.5\,\text{mm}$. It can be seen that the differences between viscous images (on the left) and inviscid images (on the right) are very small.

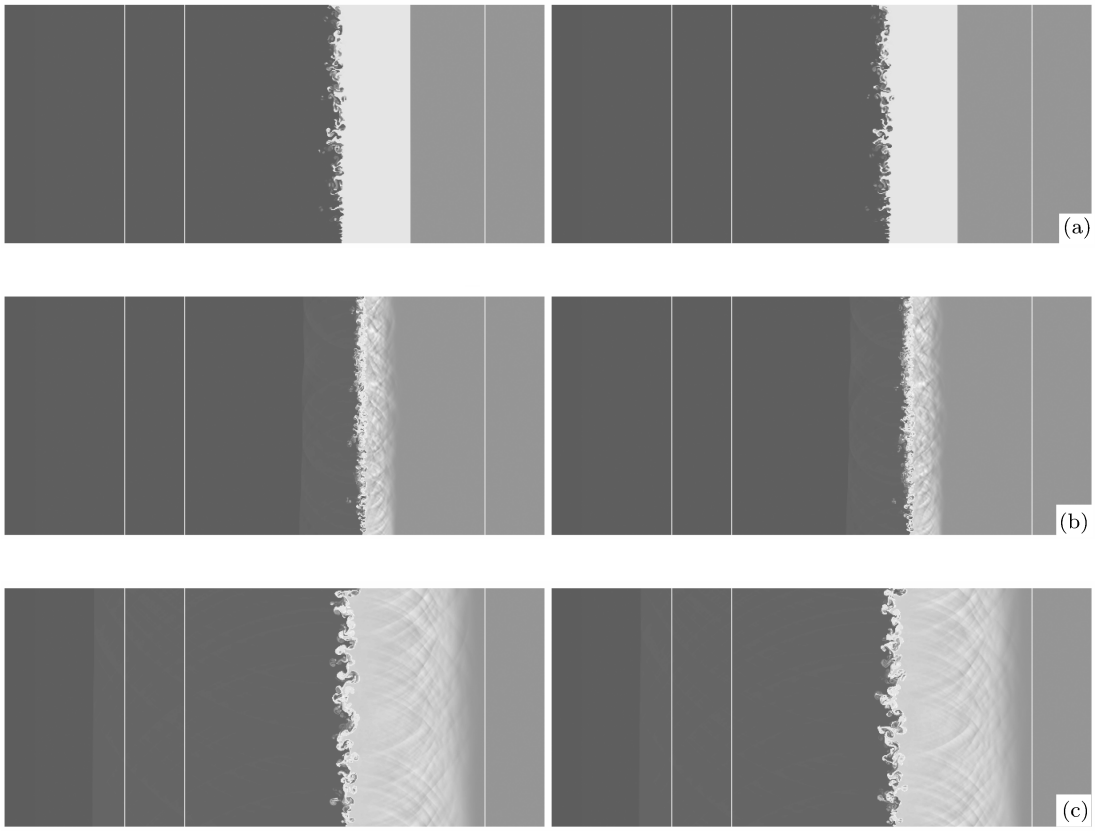


Fig.6. Configurations of density from numerical simulations for initial average wave-length $\langle\lambda\rangle$=3.5 mm. (a) t=0.087 ms, (b) t=0.013 ms, (c) t=0.113 ms.

3.3. Case 3: hydrodynamic instability and mixing of jelly model

In the jelly experiments, the jelly layer on which a periodic initial perturbation is exerted is accelerated by explosion products of a gaseous explosive mixture (GEM), i.e. C_2H_2 and O_2. The initial perturbation is located on the interface between the GEM and jelly layer, the perturbation equation is $x = \eta\cos(2\pi y/\lambda)$, where η and λ are amplitude and wavelength respectively, and the experimental and computational model is presented in Fig.7. The air is ideal gas. The jelly is mainly made of water, so its initial density is about $1000\,\text{kg/m}^3$, and the pressure is $1.013\times10^5\,\text{Pa}$, the ra-

tio of specific heat γ is 7.0. The exploding process of GEM with an 1.823×10^6 Pa instantaneous explosion pressure and $\gamma = 2.5$ can be neglected, because it is very transitory. The grid resolution is 0.2 mm. All boundaries are walls except right one. The periodic initial perturbation has three forms:

(1) η_1=0.5 mm, and λ_1=8 mm;

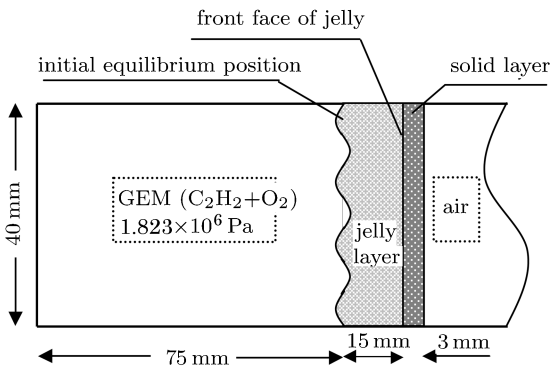


Fig.7. Experimental and computational model.

(2) η_2=1.0 mm, and λ_2=8 mm;

(3) η_3=1.0 mm, and λ_3=5 mm.

In the simulations, the displacements of front face of jelly layer X_1, top of bubble X_2 and spike head X_3, relative to the initial equilibrium position, are given, and the sketch map of X_1, X_2, X_3 is displayed in Fig.8.

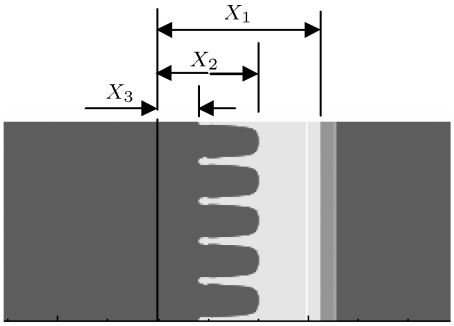


Fig.8. Sketch map of X_1, X_2 and X_3.

Figures 9(a)–9(b) show the displacements X_1, X_2, X_3 versus time for three kinds of initial perturbations,

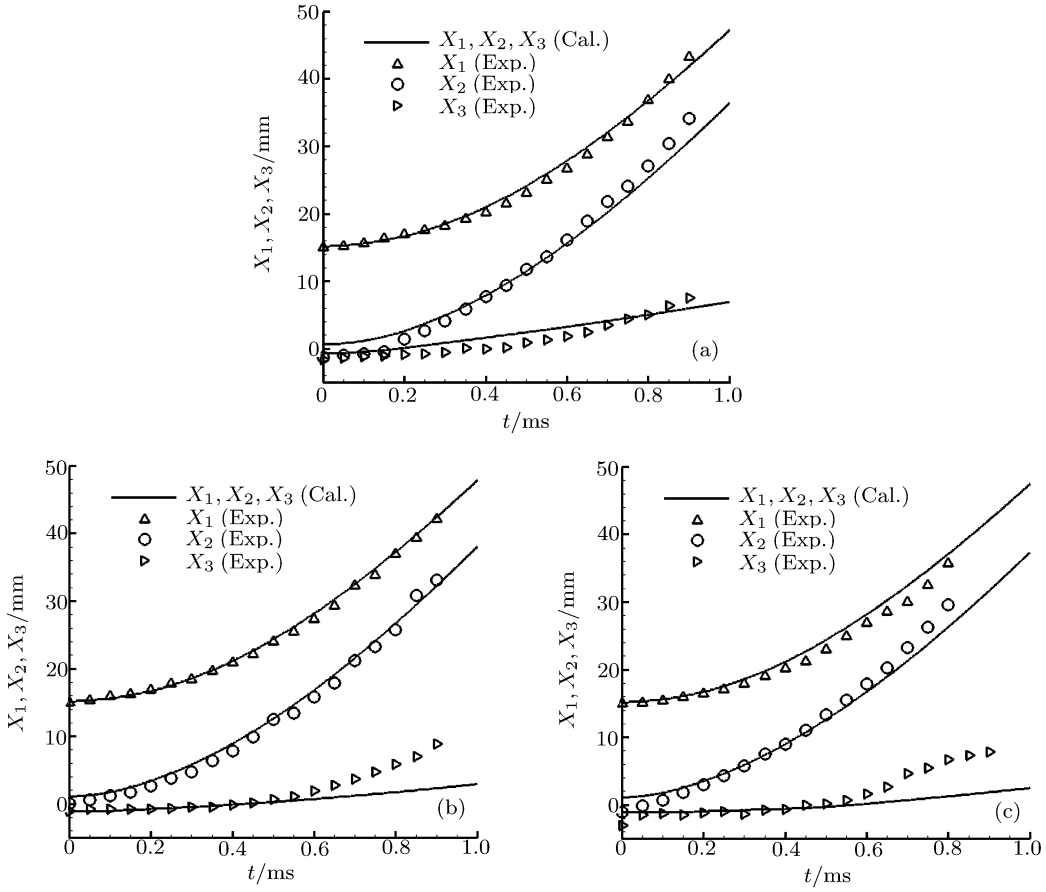


Fig.9. (a) X_1, X_2 and X_3 vs time with $\eta_1 = 0.5$ mm, and $\lambda_1 = 8$ mm; (b) X_1, X_2 and X_3 vs time with $\eta_2 = 1.0$ mm, and $\lambda_2 = 8$ mm; (c) X_1, X_2 and X_3 vs time with $\eta_3 = 1.0$ mm, and $\lambda_3 = 5$ mm.

and a comparison between numerical and experimental results, revealing that all the numerical results are in good agreement with the experimental results except the displacement X_3. For the displacement X_3, numerical results are in good agreement with experimental data at the early time, but deviate from them at the late time. In the calculations, the jelly is treated as a fluid and the shearing strength is not taken into consideration. Besides, the influence of material intensity on spike growth rate is larger than on bubble growth rate but slight on the moving speed of front face of jelly layer as a whole. For different initial perturbations, the experimental results show small differences, whereas the spike grows faster in numerical simulation when $\eta = 1.0\,\mathrm{mm}$, and the amplitude of initial perturbation is a key factor to influence the evolution of interface. Figures 10(a)–10(c) show the images of experimental measurements and numerical simulations of GEM/jelly interface at three times. The configurations are consistent with each other on the whole, the evolution of interface in simulation is more regular because of ideal state considered in calculations.

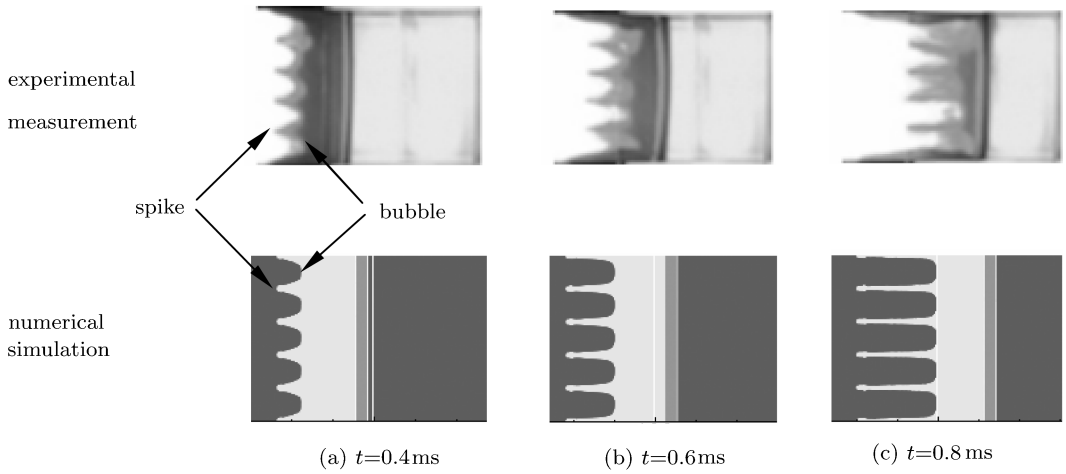


Fig.10. Configurations of GEM/jelly interface with $\eta_1 = 0.5\,\mathrm{mm}$ and $\lambda_1 = 8\,\mathrm{mm}$.

4. Summary

In this paper, the multi-viscosity-fluid hydrodynamic code MVPPM is developed and used to study the instability and the flow mixing under the impaction of shock waves. And good results are achieved.

(1) The code MVPPM is verified and validated in the case of instability under the impaction of reshocks, and the numerical results are in good agreement with experimental measurements when initial perturbation spectra contain a large enough wavelength ($\langle\lambda\rangle = 3.5\,\mathrm{mm}$).

(2) The experiments of jelly layer driven by the GEM explosion are simulated, good agreement with the measurements is achieved except for the displacement of spike head X_3 at the late time, which is perhaps because the jelly intensity is ignored. Besides, the amplitude of initial perturbation is an important factor influencing the evolution of interface.

(3) In the future work, the shearing strength should be considered and the elastic plastic model should be adapted to the description of the condensed phase. In simulations, what should be taken into account is not only the molecular dynamic viscosity, but also the turbulent kinetic viscosity, because of its important role in hydrodynamic instability and turbulent mixing.

References

[1] Richtmyer R D 1960 *Commun. Pure Appl. Math.* **13** 297
[2] Meshkov E E 1970 *NASA Tech. Trans.* **F-13** 74
[3] Rayleigh L 1900 *Scientific Papers* (Cambridge: Cambridge University Press) **2** p200
[4] Taylor G I 1950 *Proc. R. Soc. London* A **201** 192
[5] Sharp D H 1984 *Physica* D **12** 3

[6] Haas J F and Sturtevant B 1987 *J. Fluid Mech.* **181** 41

[7] Glimm J, Li X L, Menikoff R, Sharp D H and Zhang Q 1990 *Phys. Fluids* A **2** 2046

[8] Jacobs J W 1993 *Phys. Fluids* A **5** 2239

[9] Rightley P M, Vorobieff P and Benjamin R F 1997 *Phys. Fluids* **9** 1770

[10] Holder D A, Smith A V, Barton C J and Youngs D L 2003 *Laser and Particle Beams* **21** 411

[11] Kumar S, Vorobieff P, Orlicz G, Palekar A, Tomkins C, Goodenough C, Marr-Lyon M, Prestridge K P and Benjamin R F 2007 *Physica* D **235** 21

[12] Jacobs J W and Sheeley J M 1996 *Phys. Fluids* **8** 405

[13] Bai J S, Li P, Wang T, Xie B, Zhong M and Chen S H 2007 *Explosion and Shock Waves* **27** 515 (in Chinese)

[14] Bai J S, Li P and Tan D W 2006 *Chin. Phys. Lett.* **23** 1850

[15] Bai J S, Li P, Tan D W and Jiang Y 2007 *Acta Mech. Sin.* **39** 741 (in Chinese)

[16] Hankin K S R 2001 *J. Comput. Phys.* **172** 808

[17] Hirt C W and Nichols B D 1981 *J. Comput. Phys.* **39** 201

[18] Lafaurie B, Nardone C, Scardovelli R, Zaleski S and Zanetti G 1994 *J. Comput. Phys.* **113** 134

[19] Shi H H and Kishimoto Masami 2003 *Explosion and Shock Waves* **23** 391 (in Chinese)

[20] Leinov E, Formoza A, Sadot O, Yoself-Hai A, Malamud G, Elabz Y, Levin A, Shvartz D and Ben-Dor G 2006 10*th IWPCTM* Paris, France p188

[21] Malamud G, Elabz Y, Leinov E, Formoza A, Sadot O, Shvartz D and Ben-Dor G 2006 10*th IWPCTM* Paris, France p215

[22] Zhang Q and Graham M J 1998 *Phys. Fluids* **10** 974

[23] Yan Ch L, Sun D J, Yin X Y and Tong B G 2001 *Chin. J. Comput. Phys.* **18** 27 (in Chinese)